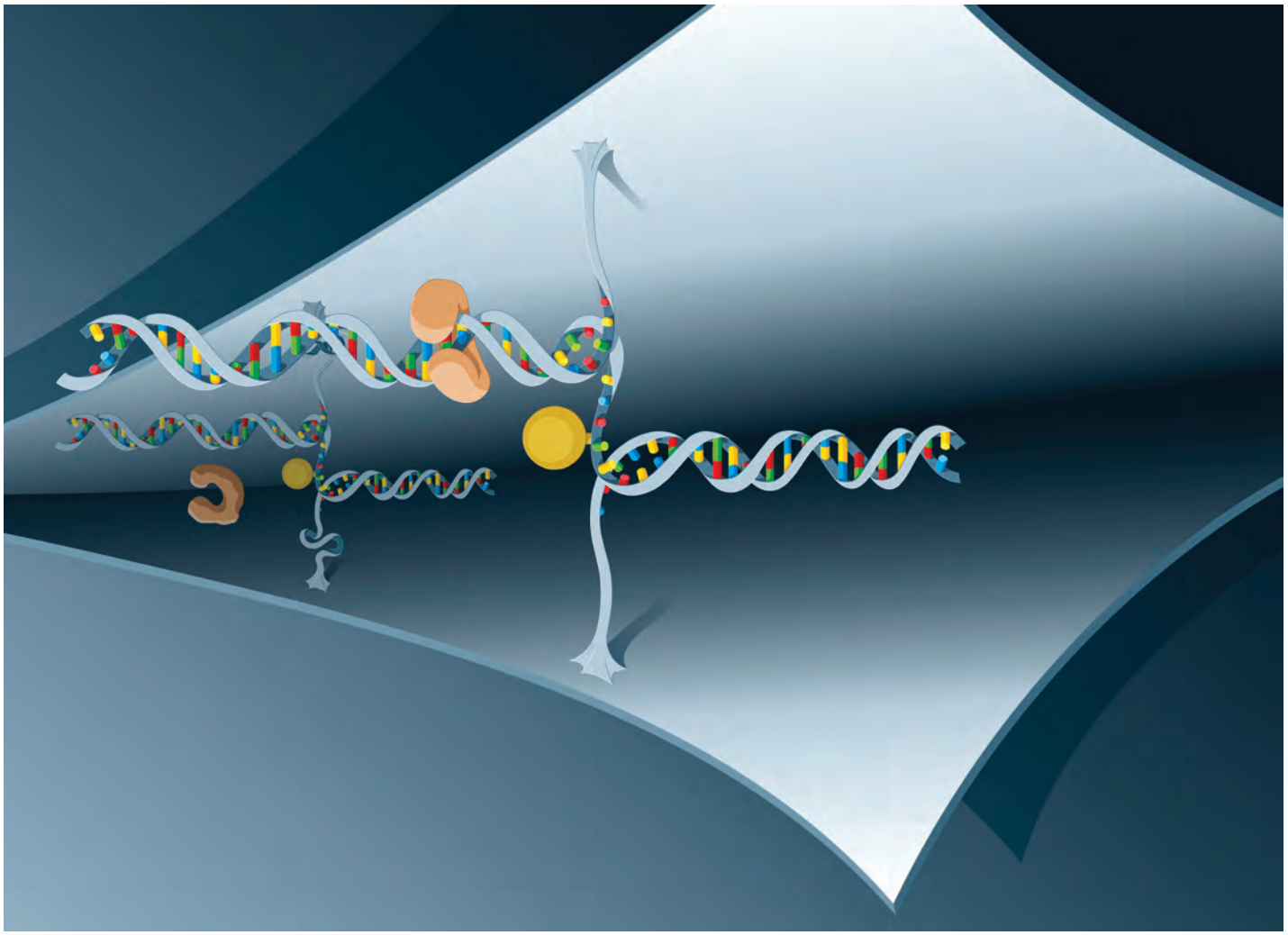

Featuring work from the Single Molecule Biophysics Laboratory of Hermann E. Gaub, Center for Nano-Science, Ludwig-Maximilians-Universität München, Germany.

Title: Protein–DNA force assay in a microfluidic format

Protein–DNA interaction forces are studied using a miniaturized and multiplexed molecular force assay on a microfluidic MITOMI chip and with a new confocal analysis method.

As featured in:

See Marcus Otten *et al.*, *Lab Chip*, 2013, **13**, 4198.

RSC Publishing

www.rsc.org/loc

Registered Charity Number 207890

Lab on a Chip

RSC Publishing

PAPER

View Article Online
View Journal | View Issue

Protein–DNA force assay in a microfluidic format†

Marcus Otten, Philip Wolf and Hermann E. Gaub

Cite this: *Lab Chip*, 2013, **13**, 4198

Received 12th July 2013,
Accepted 2nd August 2013

DOI: 10.1039/c3lc50830g

www.rsc.org/loc

The detailed study of protein–DNA interactions is a core effort to elucidate physiological processes, including gene regulation, DNA repair and the immune response. The molecular force assay (MFA) is an established method to study DNA-binding proteins. In particular, high-affinity binder dissociation is made possible by the application of force. Microfluidic lab-on-a-chip approaches have proven helpful for parallelization, small sample volumes, reproducibility, and low cost. We report the successful combination of these two principles, forming a microfluidic molecular force assay and representing a novel use for the established MITOMI chip design. We present, characterize, validate and apply this integrated method. An alternative confocal fluorescence microscopy readout and analysis method is introduced and validated. In a multiplexing application, EcoRI binding is detected and characterized. This method paves the way for quantitative on-chip force measurements. It is suited for integration with DNA micro-spotting and *in vitro* expression of transcription factors to form a high-throughput chip for detailed DNA–protein interaction studies.

Introduction

DNA–protein studies

Interactions between proteins and DNA are ubiquitous in living systems. Most prominently, DNA-binding transcription factors regulate gene expression.[1] Furthermore, proteins are involved in DNA repair[2,3] and the immune response.[4] In each of these tasks, the binding process and forces involved are crucial for function and can only be understood by combining a range of measurements, including affinity,[5] specificity,[6,7] turnover[8] and binding force.[9] As a most prominent example, transcription factor binding and turnover dynamics are a better predictor for functional regulation than mere occupancy levels.[10] A variety of methods for measuring DNA–protein interactions have been proposed, which differ most notably in measurement environment (*in vivo versus in vitro*), in washing requirements, in labeling needs, and in multiplexing capabilities. Chromatin-immunoprecipitation (ChIP)-based methods[11] have proven very valuable for *in vivo* measurements, despite the need for specialized antibodies for precipitation. Protein-binding microarrays (PBM)[12,13] are well suited to detect high affinity binding sequences for a given protein, if available in high amounts. Yeast-one-hybrid (Y1H)[14,15] and bacterial one-hybrid (B1H)[16] approaches are typically used to determine the proteins that bind to a given DNA sequence and are thus complementary to ChIP and PBM. High-throughput versions have been proposed.[17] These methods have a common set of drawbacks, including the need for labeling antibodies, low sensitivity or resolution and lack of parallel screening of multiple DNA sequences against multiple proteins and multiple references. This highlights the need for integrated methods, which will help overcome these drawbacks.

The molecular force assay

The molecular force assay (MFA) is an established method to probe intermolecular bonds, *e.g.* DNA–protein interactions. A probe bond and a known reference are assembled in series on a surface, bond-breaking forces are applied *via* surface retraction and a fluorescence readout reveals the bond rupture site. This approach has numerous advantages, including high sensitivity, statistical significance, its ability to detect both weak and strong binders and its independence of binder labels. Its sensitivity is due to the use of single molecules as the reference force sensor. Statistics are readily assembled in a single run, because many bonds are probed in parallel on a surface. By tuning the reference bond *via* its length, one can adapt to binders of varying strength. The active force load upon surface retraction speeds up unbinding of strong binders, up to dissociation constants in the pM range. The force probe DNA oligomers are labeled and used for the fluorescent readout, but these fluorophores are not directly at the probe or binding sites. The binder is not labeled. MFA has been used for a variety of applications and alterations of the DNA, including mismatches,[18] methylation[19] or hydroxymethylation[20] have been shown to be detectable. Its measurement principle has been applied to the binding of transcription factors, nucleases and polyamides[21] and RNA–protein interactions.[22]

Lehrstuhl für Angewandte Physik and Center for Nanoscience (CeNS), Ludwig-Maximilians-Universität, Amalienstrasse 54, 80799 Munich, Germany

† Electronic supplementary information (ESI) available. See DOI: 10.1039/c3lc50830g

Microfluidics and MITOMI

The advent of microfluidics and lab-on-a-chip technologies has recently spurred miniaturization and parallelization of tried-and-tested methods. Advantages include smaller sample volumes, higher throughput, facilitated reproducibility and reduced experimental time. One particular variant of microfluidics involves the use of multi-layer soft lithography, as pioneered by Quake *et al*.[23] One layer, the flow layer, can be used for biochemical reactions, whereas another is used to control these flows by application of pneumatic pressure. With respect to the study of protein–DNA interactions, Maerkl and Quake applied these design principles to obtain what is now known as the MITOMI chip, acronym for mechanically induced trapping of molecular interactions.[24] A button valve is used to seal and protect the sample area from contamination by neighbors or from stringent washing.[25] The chip has been applied to measure a variety of other interactions, including protein–protein[26] and protein–RNA.[27] In some cases, reaction chambers have been used for *in vitro* expression of the proteins to be probed.[26] Recently, the chip design has been improved for fast response times and the chip is now capable of recording association and dissociation traces.[28]

In the present publication, we introduce a novel method, which for the first time combines the MFA measurement principle with a microfluidic design. In particular, the button valve of the MITOMI chip is used to apply the force necessary for bond rupture. We characterize the setup, validate it by comparison to non-microfluidic measurements, introduce a novel readout and analysis route and apply it to detect a model binder, the endonuclease EcoRI, which shows no nuclease activity in the absence of its cofactor Mg^{2+}.

Results & discussion

Method summary

The microfluidic chip design is identical to the 640-chamber MITOMI chip introduced by Maerkl and Quake.[24] The chips are produced by two-layer soft lithography of polydimethylsiloxane (PDMS). The inner walls of the flow layer display covalently attached DNA duplexes after a series of treatments

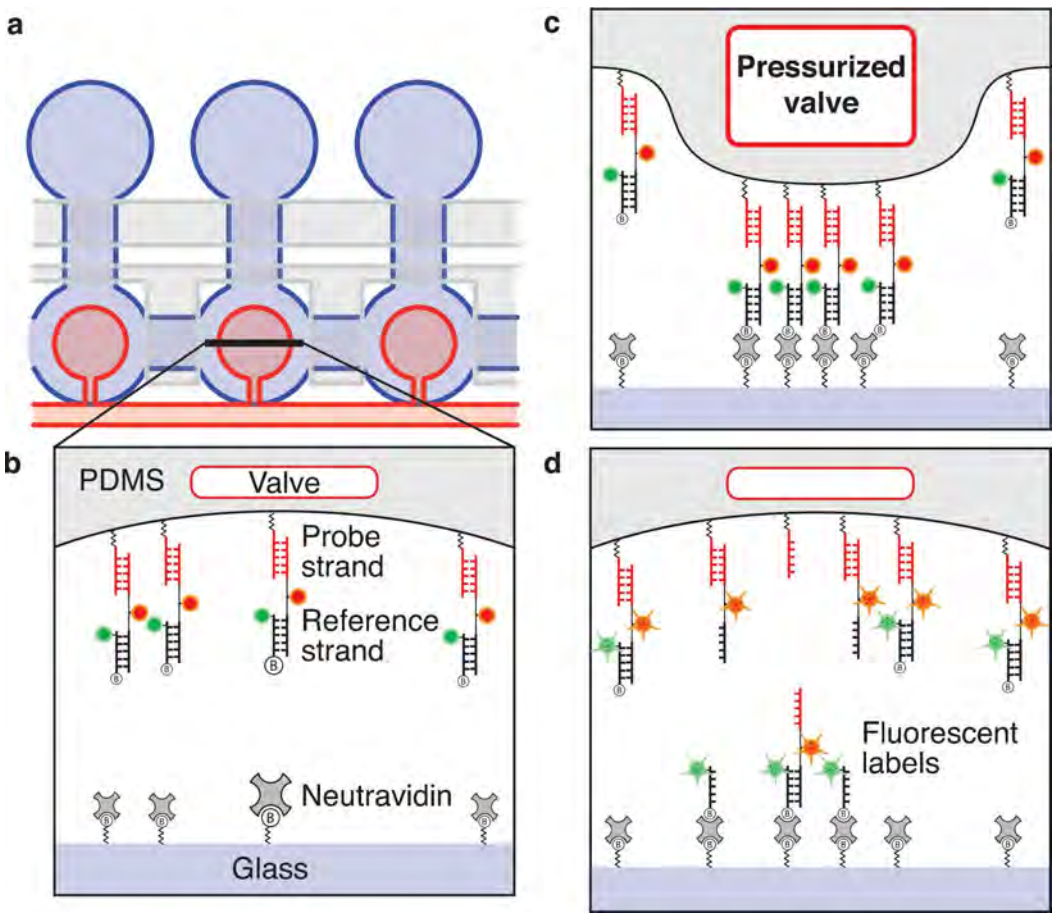

Fig. 1 Experimental design. (a) shows three of 640 double chambers in the flow layer (blue) and the overlying control layer valves (red and grey), which can expand into the flow layer by pneumatic pressure. (b) shows the initial distribution of PEG–biotin–neutravidin complexes at the glass surface and PEG–DNA probe–fluorophore–biotin complexes along the flow layer PDMS wall. (c) Actuation of the button valve establishes contact between the glass and PDMS surfaces within the button valve region only. (d) After pressure release and button retraction, the fluorophore distribution is recorded on a confocal fluorescence readout. Transferred Cy3 fluorophores (green) denote the coupling efficiency, whereas transferred Cy5 (red) is a measure of the force probes broken at the top DNA duplex bond.

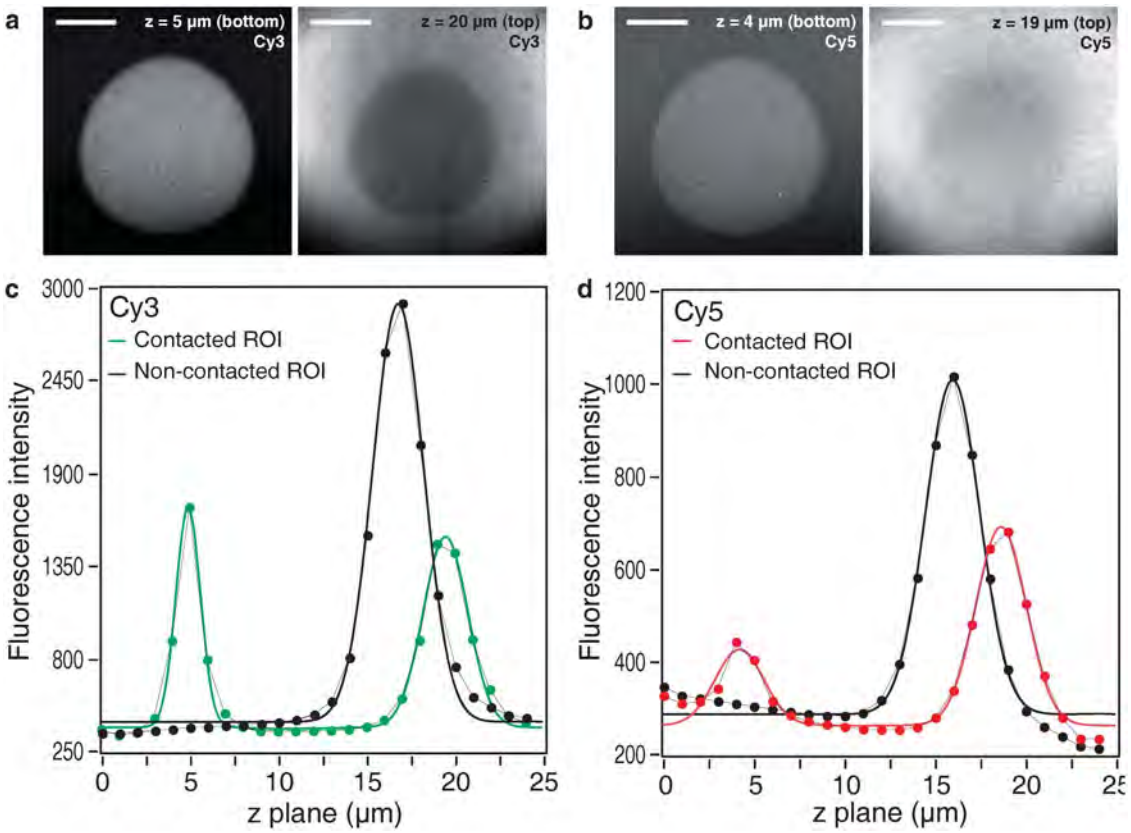

Fig. 2 Single-chamber data readout. (a) and (b) show fluorescence images of the Cy3 and Cy5 channels, respectively. The bottom glass surface slices and top PDMS surface slices are shown after button retraction. The bottom slices show transferred fluorophores and DNA strands, which are missing from the top surfaces. Scale bar: 25 µm. (c) and (d) show the vertical intensity profiles of the Cy3 and Cy5 channels, respectively. The mean intensity of the two regions of interest (ROI) is computed and plotted (dots) against the *z* slice position and fitted with Gaussian functions (lines). The contacted ROI (under the button valve) data is shown in color (green or red), the non-contacted ROI (to the side of the chamber) is shown in black. The Gaussian fit data serve for all follow-up analysis. The vertical shifts between the contacted and non-contacted ROI data are due to the PDMS chamber curvature.

with hydrochloric acid, aminosilane, NHS–polyethylene glycol–maleimide, and thiolized DNA oligomers[29,30] (Supplemental Fig. 1, ESI†). After bonding the functionalized chip to a neutravidin-coated glass slide, the button valve of the PDMS control layer is actuated by a linear pressure increase. Upon button retraction, one of the bonds will give, according to their relative rupture probabilities. The relative fluorophore distributions (top *vs.* bottom surfaces, or contacted *vs.* non-contacted regions) are determined by confocal fluorescent microscopy and analyzed to determine the relative rupture probabilities of the DNA duplex bonds (Fig. 1). The Cy3 transfer is proportional to the coupling efficiency of the biotin–neutravidin bond, whereas the location of the Cy5 signal reveals the stronger bond. For a more detailed description of the experimental workflow, we refer to the ESI†.

MFA principle & characterization

Fig. 1 shows the experimental design and measurement principle of the MFA. Each of the 640 chambers of the MITOMI chip displays two DNA duplexes in series at the top PDMS surface. The known bond will serve as a reference whereas the other one is the probe. By actuation of the button valve, a circular region is brought into contact with the glass surface underneath and coupling occurs *via* biotin–neutravidin interactions. Upon pressure release and button retraction, both duplexes are probed under force and one of them ruptures, with probabilities related to their relative strengths.[31] The fluorophores attached to strands 2 and 3 allow for their localization by confocal fluorescence imaging.

We characterize the button valve actuation by reflection interference contrast microscopy. The spatial succession of the interference maxima and minima reveals the shape of the PDMS button just prior to glass contact. We find the surface to be parabola-shaped with high reproducibility. The temporal succession of the interference maxima and minima reveals the approach and retraction velocities of this surface perpendicular to the glass surface. The approach and retraction speed can be controlled by variation of the pressure slope. In the present publication, this slope was chosen to be 0.1 psi s^{-1}, ensuring an equal valve actuation across all chambers and chips. We find good agreement between the approach velocity of 0.23 µm s^{-1}, and the retraction velocity of 0.26 µm s^{-1}, independent of the radial distance from the parabola tip (Supplemental Fig. 2, ESI†). These values are compatible with the low speeds of the piezoelectric actuator used in previous MFA implementations between 0.2 and 20 µm s^{-1}.

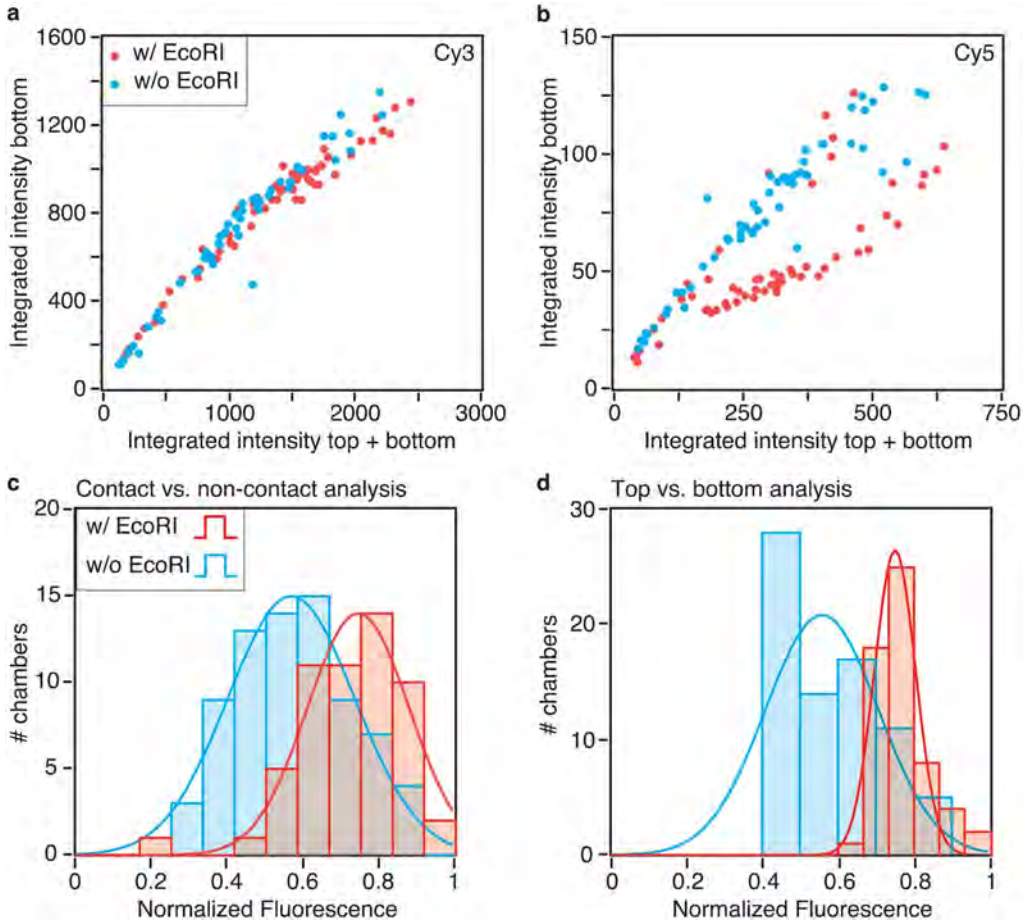

Fig. 3 Chip analysis. (a) and (b) show scatter plots of Cy3 and Cy5 intensity data from hundreds of chambers, respectively. For each chamber the integrated bottom signal is plotted against the sum of its integrated bottom and top signals in the contacted ROI only. (c) and (d) show histograms of the normalized fluorescence (corresponding to the relative bond rupture probability) computed using the contact-*vs.*-non-contact and top-*vs.*-bottom analysis methods, respectively. The histograms are fitted with Gaussian distributions. The histograms and fits are shown with and without the presence of EcoRI binders (red and blue, respectively).

Multiple key differences to previous MFA implementations emerge. First, the force application occurs by pneumatic means, rather than by a voltage-controlled piezo element. No bulk PDMS can dampen the retraction movement, which allows more direct control of the retraction speed. Second, the contact and separation occurs between a flat glass surface and a rounded PDMS surface, as opposed to two planar surfaces. This is predicted to be a more favorable geometry to avoid non-linear retraction effects. Soft lithography and photoresist reflow are versatile tools to tune the actuation of this membrane.[32] Third, the small distance separating the two fluorescent surfaces facilitates comparable readouts of both surfaces. Previously, only the glass surface was analyzed. This additional set of data opens up a top-*vs.*-bottom analysis route, rather than the traditional contact-*vs.*-non-contact method.

Comparison of analysis methods

The data readout and analysis for a single chamber are shown in Fig. 2. Confocal scans are performed identically for two fluorescent channels, Cy3 and Cy5. The Cy5 signal is a measure of the number of transferred middle strands, whereas the Cy3 signal is a measure of the coupling efficiency of the probe *via* biotin–neutravidin bonding to the glass surface. The contacted region of interest (ROI) beneath the button valve shows fluorescence signals both at the glass surface and at the PDMS surface, whereas the non-contacted ROI shows no fluorescence transfer from the PDMS onto the glass surface, as can be seen in Fig. 2c and 2d. Both distributions can be fitted with Gaussian functions. This data collection opens up two alternative analysis routes: (1) a contact-*vs.*-non-contact method similar to the previously introduced MFA analysis, and (2) a top-*vs.*-bottom method. The first compares the two regions at the PDMS surface to determine the missing dye fraction at the contacted ROI, whereas the second method compares the two peaks of the contacted ROI to determine the transferred dye fraction.

The quantity of interest is the relative rupture probability of the two bonds. On the basis of previous MFA studies, it is named "normalized fluorescence" (NF) and denotes the fraction of probes ruptured at the lower bond, normalized to the number of probes coupled and under load. It is thus equivalent to the relative rupture probability of the two bonds. It can be expressed as follows for the contact-*vs.*-non-contact

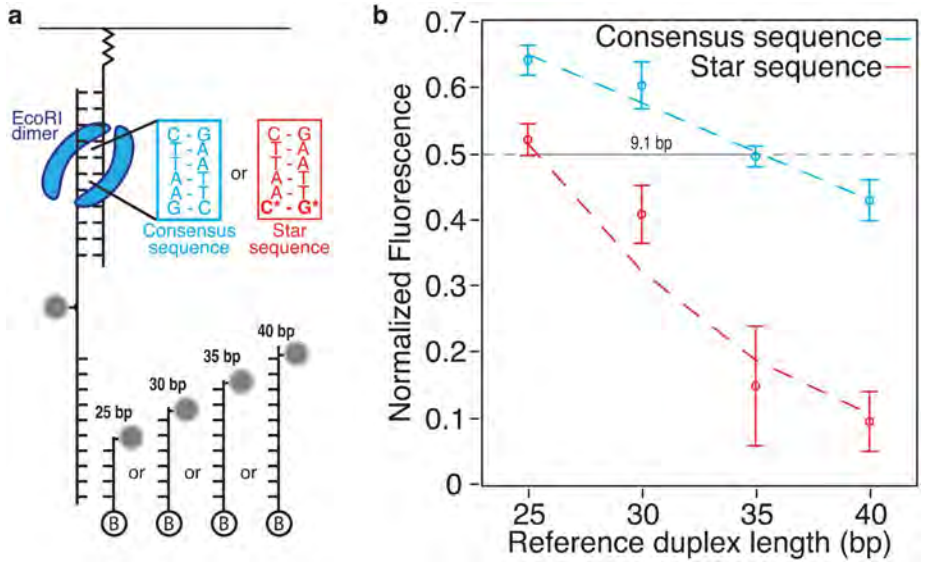

Fig. 4 Multiplexing application. (a) shows the multiplexed design of DNA strands to form molecular force probes displaying either the EcoRI consensus sequence GAATTC (blue) or the star sequence GAATTG (red) and to be probed against references of varying lengths (25–40 bp). Each construct is flushed into a separate microfluidic row on the same chip. (b) shows the dependence of the median normalized fluorescence in the case where EcoRI is presented to the probes shown in (a). The drop in NF upon sequence variation (from consensus to star) and upon reference elongation characterizes the specific binding and mechanical stabilization by EcoRI. The experimental results (circles, error bars) can be fitted with a Bell–Evans model simulation (dashed lines) with very good agreement.

analysis:

$$\mathrm{NF} = \frac{\dfrac{\mathrm{Cy5}_\mathrm{t}^\mathrm{c}}{\mathrm{Cy5}_\mathrm{t}^\mathrm{nc}} - \dfrac{\mathrm{Cy3}_\mathrm{t}^\mathrm{c}}{\mathrm{Cy3}_\mathrm{t}^\mathrm{nc}}}{1 - \dfrac{\mathrm{Cy3}_\mathrm{t}^\mathrm{c}}{\mathrm{Cy3}_\mathrm{t}^\mathrm{nc}}}$$

and for the top-*vs.*-bottom method:

$$\mathrm{NF} = 1 - \frac{\dfrac{\mathrm{Cy5}_\mathrm{b}^\mathrm{c}}{\mathrm{Cy5}_\mathrm{t}^\mathrm{c} + \mathrm{Cy5}_\mathrm{b}^\mathrm{c}}}{\dfrac{\mathrm{Cy3}_\mathrm{b}^\mathrm{c}}{\mathrm{Cy3}_\mathrm{t}^\mathrm{c} + \mathrm{Cy3}_\mathrm{b}^\mathrm{c}}}$$

with the following notation: $\mathrm{channel}_{\mathrm{location}}^{\mathrm{region}}$, where channel is either Cy3 or Cy5, region is either c (contacted) or nc (non-contacted), and location is either t (top) or b (bottom). All intensity values are computed by integration of the respective Gaussian fit curves (background excluded). The two analysis routes are evaluated for consistency. Considering bare DNA probes in the absence of binders, we obtain a median normalized fluorescence of 0.56 ± 0.03 (s.d.) for the contact-*vs.*-non-contact analysis and of 0.55 ± 0.03 for the top-*vs.*-bottom method. The slight deviation from the symmetric distribution can be attributed to different polyethylene glycol linker lengths at the glass and PDMS surfaces. Furthermore, the fluorescence dyes are expected to show excitation and emission characteristics dependant on the local environment, which differ at the glass and the PDMS surfaces.[33] This very good agreement underlines the equivalency of the two analysis methods. The top-*vs.*-bottom analysis route is possibly less prone to errors. Uneven illumination, inhomogeneous surface functionalization and optical effects are excluded as possible sources of error. Previously, these were corrected for by taking an additional set of images at the beginning of the experiment. In particular for high-throughput implementations, this leads to a longer experiment time and to fluorophore bleaching.

EcoRI detection

An exemplary demonstration of the DNA–protein binding detection by MFA is the effect of EcoRI binding, in the absence of its nuclease cofactor. The top DNA duplex contains the palindromic consensus sequence 5′-GAATTC-3′. Upon binding, we expect the consensus sequence to be strengthened and the rupture probabilities to shift towards the non-binding reference duplex. Fig. 3 shows the effect of EcoRI binding for a single, representative chip with statistics from 140 chambers. While the coupling efficiency, determined by the fraction of transferred Cy3 fluorophores, is not affected (Fig. 3a), the transfer of Cy5-containing middle strands is reduced in the presence of EcoRI (Fig. 3b). These differences in transfer translate into shifted distributions of normalized fluorescence values. For the contact-*vs.*-non-contact analysis method, the median of the chambers shifts from 0.56 to 0.73 (Fig. 3c). For the top-*vs.*-bottom analysis method, it shifts from 0.54 to 0.75 (Fig. 3d). These values are in good agreement with each other. Literature values from previous MFA studies with 20 bp oligomer samples and references show the same trend, with slightly differing absolute values, namely an increase from 0.48 to 0.62.[21] However, these differences may be explained by the oligomers' differences in length and in G/C content.

Multiplexing

The row-by-row multiplexing capabilities of the present experimental design are assessed by measuring EcoRI binding onto two different binding sequences (the EcoRI consensus sequence 5′-GAATTC-3′, and the star sequence 5′-GAATTG-3′) against four reference strands of varying lengths between 25

and 40 base pairs, on the same chip. Statistical significance for all 8 combinations is aimed for by preparing multiple chambers with the same combination of probe and reference. The variation of the normalized fluorescence dependent on the reference duplex length and the binding sequence composition is shown in Fig. 4. A drop in NF for increasing reference duplex length is indicative of a decreasing fraction of probes rupturing at the reference duplex. This observation is consistent with expectations and previous studies.[21] At the same time, the consensus sequence probe shows consistently higher NF values at all reference lengths, which indicates a more stable top duplex, in accordance with the expected higher binding affinity.[34,35] The data shown in Fig. 4 facilitates the quantitative understanding of the difference in EcoRI binding between its consensus and star sequences. At an equilibrated rupture probability of NF = 0.5, the mechanical stabilizing action of EcoRI binding to its consensus sequence is equivalent to an addition of 9.1 bp dsDNA in the reference strand. This analysis is supported by the very good agreement of the experimental results with a fit based on the Bell–Evans model.[36]

Conclusion

In the present publication, we have introduced a versatile method for the quantification of DNA–protein interactions, based on the application of pneumatic forces in a microfluidic chip. Upon force load, the relative rupture probabilities of two molecular bonds in series are determined by confocal fluorescence readout. We have characterized the method, with respect to the geometry and dynamics of the button valve. The method was validated with a known all-DNA probe. Then, we have introduced and validated an alternative analysis route, based on the comparison of the fluorophore distributions at the top and bottom surfaces of the sample chamber. Finally, we have applied the method to the study of EcoRI binding. This application involving multiple target and reference strands has illustrated the multiplexing capabilities of the setup. EcoRI was used as a model protein in this proof-of-principle experiment. It can readily be substituted, thus paving the way for studies of currently unknown protein–DNA interactions, including those of transcription factors. In particular, the binding forces of transcription factors were found to correlate strongly with functional regulation, more strongly even than occupancy levels.[10] Therefore, it is very promising to use the presented method with various protein variants and/or binding sequences. The multiplexing capabilities of the setup can be further expanded. DNA array microspotting technology has been shown to be compatible with the MFA without loss of validity.[21] One can choose to spot different binding and/or reference sequences. The chip also features back chambers for the spotting of cDNA plasmids or PCR products and for the expression of DNA binding protein. This on-chip expression will further increase multiplexing.

Acknowledgements

We thank S. R. Quake and M. Meier for invaluable help in setting up the microfluidic chip production and operation. We thank D. Aschenbrenner, K. Limmer, and P. Severin for helpful discussions. M. O. is grateful to the Elite Network of Bavaria (IDK-NBT) for a doctoral fellowship. This work was supported by the European Research Council.

References

1 A. Ozdemir and A. Stathopoulos, *Nat. Methods*, 2011, **8**, 1016–1017.
2 J. Jiricny, *Nat. Rev. Mol. Cell Biol.*, 2006, **7**, 335–346.
3 S. P. Jackson and J. Bartek, *Nature*, 2009, **461**, 1071–1078.
4 V. Hornung and E. Latz, *Nat. Rev. Immunol.*, 2010, **10**, 123–130.
5 R. Nutiu, R. Friedman, S. Luo, I. Khrebtukova, D. Silva, R. Li, L. Zhang, G. Schroth and C. Burge, *Nat. Biotechnol.*, 2011, **29**, 659–664.
6 G. D. Stormo and Y. Zhao, *Nat. Rev. Genet.*, 2010, **11**, 751–760.
7 M. T. Weirauch, A. Cote, R. Norel, M. Annala, Y. Zhao, T. R. Riley, J. Saez-Rodriguez, T. Cokelaer, A. Vedenko, S. Talukder, D. Consortium, H. J. Bussemaker, Q. D. Morris, M. L. Bulyk, G. Stolovitzky and T. R. Hughes, *Nat. Biotechnol.*, 2013, **31**, 126–134.
8 T. S. Karpova, M. J. Kim, C. Spriet, K. Nalley, T. J. Stasevich, Z. Kherrouche, L. Heliot and J. G. Mcnally, *Science*, 2008, **319**, 466–469.
9 J. L. Arlett, E. B. Myers and M. L. Roukes, *Nat. Nanotechnol.*, 2011, **6**, 203–215.
10 C. R. Lickwar, F. Mueller, S. E. Hanlon, J. G. Mcnally and J. D. Lieb, *Nature*, 2012, **484**, 251–255.
11 C. E. Massie and I. G. Mills, *EMBO Rep.*, 2008, **9**, 337–343.
12 M. L. Bulyk, X. Huang, Y. Choo and G. M. Church, *Proc. Natl. Acad. Sci. USA*, 2001, **98**, 7158–7163.
13 G. Badis, M. F. Berger, A. A. Philippakis, S. Talukder, A. R. Gehrke, S. A. Jaeger, E. T. Chan, G. Metzler, A. Vedenko, X. Chen, H. Kuznetsov, C.-F. Wang, D. Coburn, D. E. Newburger, Q. Morris, T. R. Hughes and M. L. Bulyk, *Science*, 2009, **324**, 1720–1723.
14 H. Yokoe and R. R. Anholt, *Proc. Natl. Acad. Sci. USA*, 1993, **90**, 4655–4659.
15 J. J. Li and I. Herskowitz, *Science*, 1993, **262**, 1870–1874.
16 X. Meng, M. H. Brodsky and S. A. Wolfe, *Nat. Biotechnol.*, 2005, **23**, 988–994.
17 K. Hens, J.-D. Feuz, A. Isakova, A. Iagovitina, A. Massouras, J. Bryois, P. Callaerts, S. E. Celniker and B. Deplancke, *Nat. Methods*, 2011, **8**, 1065–1070.
18 C. Albrecht, K. Blank, M. Lalic-Mülthaler, S. Hirler, T. Mai, I. Gilbert, S. Schiffmann, T. Bayer, H. Clausen-Schaumann and H. E. Gaub, *Science*, 2003, **301**, 367–370.
19 P. M. D. Severin, X. Zou, H. E. Gaub and K. Schulten, *Nucleic Acids Res.*, 2011, **39**, 8740–8751.
20 P. M. D. Severin, X. Zou, K. Schulten and H. E. Gaub, *Biophys. J.*, 2013, **104**, 208–215.
21 P. M. D. Severin and H. E. Gaub, *Small*, 2012, **8**, 3269–3273.
22 K. Limmer, D. Aschenbrenner and H. Gaub, *Nucleic Acids Res.*, 2013, **41**, e69.

23 M. Unger, H.-P. Chou, T. Thorsen, A. Scherer and S. R. Quake, *Science*, 2000, **288**, 113–116.
24 S. J. Maerkl and S. R. Quake, *Science*, 2007, **315**, 233–237.
25 J. L. Garcia-Cordero and S. J. Maerkl, *Chem. Commun.*, 2013, **49**, 1264–1266.
26 D. Gerber, S. J. Maerkl and S. R. Quake, *Nat. Methods*, 2009, **6**, 71–74.
27 L. Martin, M. Meier, S. M. Lyons, R. V. Sit, W. F. Marzluff, S. R. Quake and H. Y. Chang, *Nat. Methods*, 2012, **9**, 1192–1194.
28 M. Geertz, D. Shore and S. Maerkl, *Proc. Natl. Acad. Sci. USA*, 2012, **109**, 16540–16545.
29 N. R. Glass, R. Tjeung, P. P. Y. Chan, L. Y. Yeo and J. R. Friend, *Biomicrofluidics*, 2011, **5**, 036501.
30 J. L. Zimmermann, T. Nicolaus, G. Neuert and K. Blank, *Nat. Protoc.*, 2010, **5**, 975–985.
31 G. Neuert, C. H. Albrecht and H. E. Gaub, *Biophys. J.*, 2007, **93**, 1215–1223.
32 P. M. Fordyce, C. A. Diaz-Botia, J. L. DeRisi and R. Gomez-Sjoberg, *Lab Chip*, 2012, **12**, 4287–4295.
33 M. Levitus and S. Ranjit, *Q. Rev. Biophys.*, 2011, **44**, 123–151.
34 D. R. Lesser, M. R. Kurpiewski and L. Jen-Jacobson, *Science*, 1990, **250**, 776–786.
35 N. Y. Sidorova and D. C. Rau, *Biophys. J.*, 2004, **87**, 2564–2576.
36 E. Evans and K. Ritchie, *Biophys. J.*, 1999, **76**, 2439–2447.

Electronic Supplementary Information

Methods

Chip fabrication

Flow and control wafers were obtained from the Stanford Microfluidics Foundry, design name DTPAd, according to the 640-chamber MITOMI design from [1]. This design features 15 μm high flow channels, rounded by photoresist reflow, and a rectangular control channel cross-section for optimal valve closing operation. PDMS chips were fabricated as follows: For the control layer, a 5:1 mixture of Sylgard 184 (Dow Corning) base:curing agent was poured onto the wafer, degassed, partially cured at 80°C for 20 min. The flow layer wafer was spin-coated at 2500 rpm for 75 s with a 20:1 base:curing agent mixture of Sylgard 184 and partially cured at 80°C for 30 min. The control layers were cut out, holes were punched and control layers were aligned onto the flow layer PDMS on the flow layer wafer. Assembled chips were baked at 80°C for 90 min, cut, peeled off the flow layer wafer and holes were punched. After fabrication, PDMS chips were stored under Argon atmosphere for no more than 1 month.

Chip functionalization

The chip was bonded onto a clean glass slide at 80°C for 5 h. hydrochloric acid (12.5 %) was flushed into the chip for overnight storage in humid atmosphere. Silanization was prepared by flushing with ethanol for 20 min. A mixture of 70 % 3-Aminopropyldimethyl-ethoxysilane (ABCR), 5 % H_2SO_4, 25% ddH_2O was prepared, stirred for 1 h, mixed 1:4 with EtOH, and flowed through the chip for 30 min, followed by 10 min rinsing with ethanol. The silanization was consolidated by baking the chip at 80°C after peeling it off the glass slide. PEGylation was prepared by 30 min pre-incubation in borate buffer (50 mM sodium borate, pH 8.5) and accomplished by incubating the chip with 0.25 mg/ml NHS-PEG-Maleimide (MW 5000, Rapp Polymere), dissolved in borate buffer, and covered with a glass slip. The chip was then rinsed with ddH_2O and bonded for 30 min at 80°C onto a clean glass slide. For DNA functionalization, strand 1 (oligo sequences below) at 2 μM in coupling buffer (50 mM sodium phosphate pH 7.2, 50mM NaCl, 10 mM EDTA) was first flowed through the chip for 60 minutes, with the unused back chambers of the flow chambers sealed off using the corresponding valve. DNA oligos 2 and 3 were pre-incubated in 5x phosphate buffered saline (PBS) for 2 hours at concentrations of 2 μM (strand 2) and 4 μM (strand 3) and then flushed through the chip for 60 min. In parallel, a #1 thickness cover slip was prepared to serve as stamping counterpart: Therefore, it was amino-silanized (30 min), treated with NHS-PEG-Biotin (60 min, 0.25 mg/mL in Borate buffer, MW 3000, Rapp Polymere), and incubated with Neutravidin (60 min, 1 mg/mL in PBS), and rinsed with ddH_2O. Finally, the chip was rinsed and prepared for quick transfer onto the Neutravidin-presenting glass slide with a solution of 30 mM Trehalose and 5 ppm Tween in PBS allowed for short-term wetting and stabilization of the PDMS-surface-bound DNA oligomers. For all of these steps, flow layer pressure was kept constant at 4 psi.

Oligomer sequences

All oligomers were purchased from IBA GmbH. 5'-GAA TTC-3' is the palindromic recognition sequence of EcoRI and is displayed in the duplex of strands 1 and 2. For the all-DNA probe experiments, the following three strands were used:

Strand 1: (SH)-5'-ttttttttttt-CTG CAG GAA TTC GAT ATC AAG CTT ATC GAT-3'

Strand 2: 3'-GAC GTC CTT AAG CTA TAG TTC GAA TAG CTA C-ttttttt-5'-(Cy5)-5'-ttttttt-C GAC GTC CTT AAG CTA TAG TTC GAA TAG CTA-3'

Strand 3: Biotin-5'-ttttttttttt-TAG CTA TTC GAA CTA TAG CTT AAG GAC GTC-(Cy3)-3'

For the multiplexing experiments, the following strands were used in various combinations:

Strand 1-consensus: (SH)-5'-ttttttttttt-TAGACCGGAATGAATTCGCTTATCT-3'

Strand 1-star: (SH)-5'-ttttttttttt-TAGACCGGAATGAATTGGCTTATCT-3'

Strand 2-consensus: 3'-ATCTGGCCTTACTTAAGCGAATAGA-ttttttt-5'-(cy5)-5'-ttttttt-TTAGTAAGGGAGCATATTGCATACGTTGAGGACTTATCAG-3'

Strand 2-star: 3'-ATCTGGCCTTACTTAACCGAATAGA-ttttttt-5'-(cy5)-5'-ttttttt-TTAGTAAGGGAGCATATTGCATACGTTGAGGACTTATCAG-3'

Strand 3-25bp: Biotin-5'-ttttttttttt-CTGATAAGTCCTCAACGTATGCAAT (Cy3)-3'

Strand 3-30bp: Biotin-5'-ttttttttttt-CTGATAAGTCCTCAACGTATGCAATATGCT (Cy3)-3'

Strand 3-35bp: Biotin-5'-ttttttttttt-CTGATAAGTCCTCAACGTATGCAATATGCTCCCTT (Cy3)-3'

Strand 3-40bp: Biotin-5'-ttttttttttt-CTGATAAGTCCTCAACGTATGCAATATGCTCCCTTACTAA (Cy3)-3'

Prior to each experiment, Thiol-containing strands were reduced with 5 mM TCEP (Thermo Fischer Scientific), purified by ethanol precipitation and resuspended in coupling buffer. EcoRI was purchased from New England Biolabs and flushed into the chip at a concentration of 10 nM in a buffer solution (pH 7.6) containing 10 mM HEPES, 170 mM NaCl, 1 mM EDTA, 50 μM DTT, and 100 μg/mL BSA.

Contacting mechanism

The functionalized chip, bound to the Neutravidin glass slide, was flushed with 1x PBS at a reduced pressure of 0.5 psi prior to button actuation ("stamping") and measurement. The button valve pressure was linearly increased from 0 psi to 15 psi over 150 s. After a contact time of 10 min, the button was retracted by lowering the pressure to 0 psi linearly over 150 s.

Readout

Data acquisition was performed chamber-by-chamber, scanning the microfluidic chip. Confocal stacks of up to 25 images at a vertical distance of 1 μm were recorded

for the cy3 and cy5 channels using a spinning disk unit (Yokogawa) and an EMCCD Camera (Andor) on an inverted microscope through a 40x / 1.3 NA oil immersion objective (Carl Zeiss). The chip was scanned using hybrid DC/piezo motors (Physik Instrumente) for x- and y-directions, an objective piezo positioner (Physik Instrumente) for z-direction and a custom-designed scan software (Labview, National Instruments). Excitation lasers at 532 nm (cy3 channel) and 640 nm (cy5 channel) were used in combination with emission filters at 593 nm and 676 nm (AHF Analysentechnik). The exposure time was set to 100 ms to balance data quality and experiment duration. Thus, a 640-chamber chip can be scanned and imaged in 60-90 minutes. If time constraints apply, reducing the exposure time and/or increasing the confocal slice-to-slice distance will speed up readout at the expense of raw data signal-to-noise and fit quality.

Analysis

The recorded stacks of confocal fluorescent images were analyzed by choosing two distinct circular regions of interest (ROI): Region 1 corresponds to the button valve contact area, while region 2 does not overlap with the contact area. Vertical mean intensity profiles were plotted for each region and fluorescent channel. These profiles were fitted with the sum of two Gaussian functions and a constant background offset in the case of contacted region 1, and the sum of a single Gaussian and a constant background in the case of no-contact region 2. These Gaussian fit data yield integrated intensity values for each region, channel, and location (top/bottom). From these, relative rupture probabilities are computed, namely the value of normalized fluorescence. Its value between 0 and 1 denotes the fraction of probes under load, which rupture at the bottom bond.

Bell-Evans model

The multiplexing application data can be fitted with a Bell-Evans model simulation, as described in high detail previously [2]. In short, both the probe and reference bonds can be described by a two-state rupture probability depending on force f, force loading rate f', potential width Δx and rate k_{off}:

$$p(f,f') = \frac{k_{off}}{f'} \cdot \exp\left(\frac{f \cdot \Delta x}{k_B T}\right) \cdot \exp\left(-\frac{k_{off}}{f'} \cdot \int_0^f du \cdot \exp\left(\frac{u \cdot \Delta x}{k_B T}\right)\right)$$

Δx and $\log(k_{off})$ are assumed to be linear functions of oligomer length n:

$$k_{off} = 10^{\alpha - \beta \cdot n}\, s^{-1}$$

$$\Delta x = (t + n \cdot m) \cdot 10^{-10}\, m$$

α, β, t and m are the independent fit parameters. For dsDNA, previous experimental studies have found: $\alpha = (3 \pm 1)$, $\beta = (0.5 \pm 0.1)$, $t = (7 \pm 3)$, $m = (0.7 \pm 0.3)$[3]. The loading rate of 10^5 pN s^{-1} was estimated experimentally from PDMS stamp separation velocity, effective spring constants of the PEG linkers and the functionalization density [4]. The oligomer length dependence of normalized fluorescence is then given by:

$$NF\left(f',n_{ref},n_{probe}\right) =$$

$$= \frac{1}{2}\left[1 - \int_{fA}^{\infty} df\left(p_{ref}\left(f,f',n_{ref}\right) - p_{probe}\left(f,f',n_{probe}\right)\right) - \int_{fB}^{\infty} df\left(p_{ref}\left(f,f',n_{ref}\right) - p_{probe}\left(f,f',n_{probe}\right)\right)\right]$$

with the fA and fB, the points of equal rupture probability, defined by:

$$p_{ref}\left(fA,f',n_{ref}\right) = p_{probe}\left(fA,f',n_{probe}\right)$$

$$p_{ref}\left(fB,f',n_{ref}\right) = p_{probe}\left(fB,f',n_{probe}\right)$$

If only one force fA > 0 fulfills this requirement, then fB = 0. The fit routine yields values in consistency with literature values: α = 3.73, β = 0.355, t = 5.24, m = 0.415.

References

1. Maerkl, S.J. & Quake, S.R. A systems approach to measuring the binding energy landscapes of transcription factors. *Science* 315, 233-237 (2007).

2. Severin, P.M.D. & Gaub, H.E. DNA-protein binding force chip. *Small* 8, 3269-3273 (2012).

3. Strunz, T., Oroszlan, K., Schäfer, R. & Güntherodt, H.J. Dynamic force spectroscopy of single DNA molecules. *P Natl Acad Sci Usa* 96, 11277-11282 (1999).

4. Albrecht, C.H., Neuert, G., Lugmaier, R.A. & Gaub, H.E. Molecular force balance measurements reveal that double-stranded DNA unbinds under force in rate-dependent pathways. *Biophys J* 94, 4766-4774 (2008).

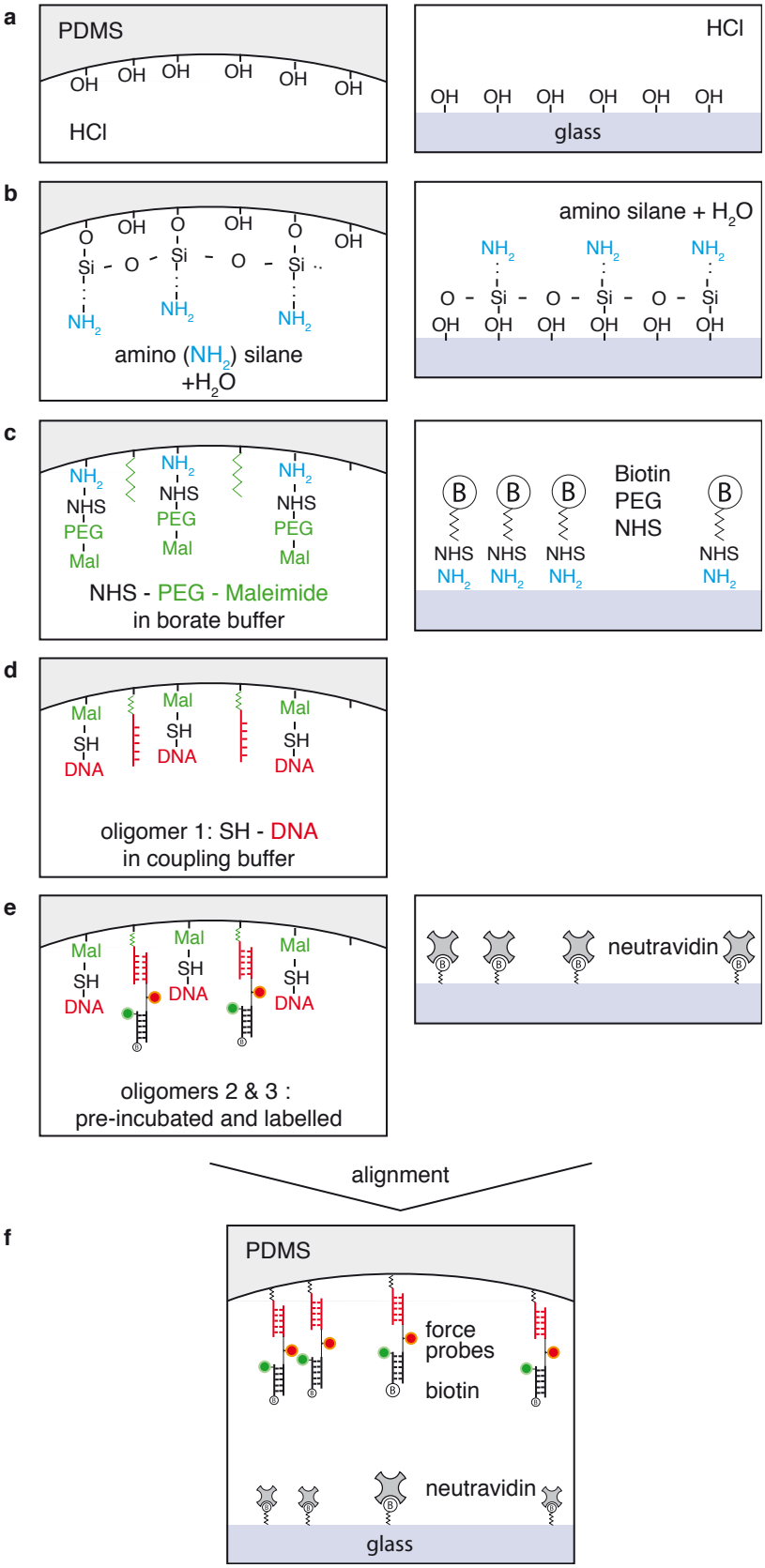

Supplemental Figure 1

Chip and slide functionalization. (a)-(e) schematically summarize the multistep functionalization procedure of chip and slide as described in the online method section. (f) shows the resulting setup after chip and slide alignment.

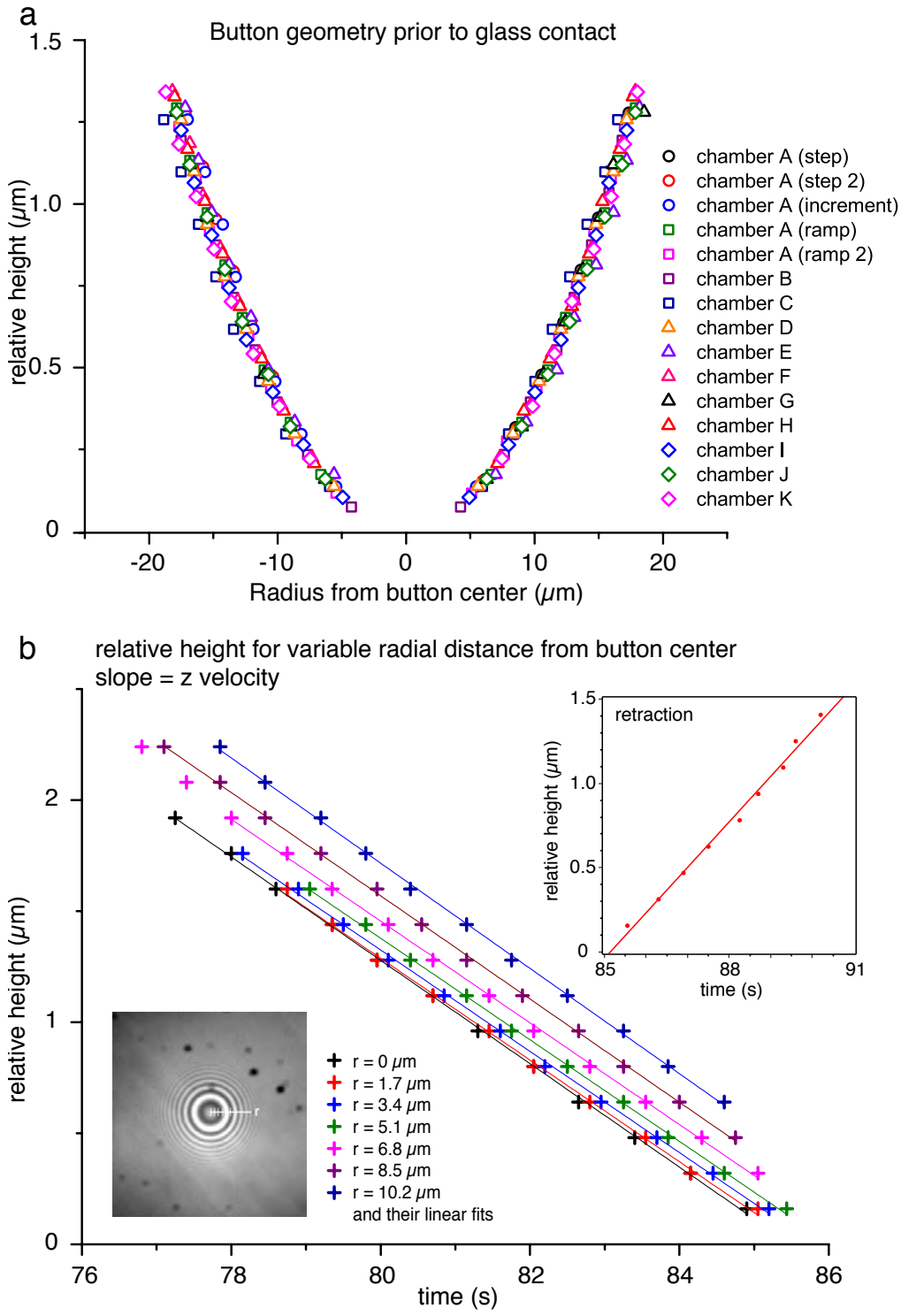

Supplemental Figure 2

Button geometry and dynamics. (a) Button geometry just prior to glass contact in multiple chambers, determined by interference patterns between glass and PDMS in microscopy. (b) PDMS-Glass distance plotted against time. Various radial distances from button valve center (cf. bottom-left inset) are plotted for approach dynamics (main graph) and compared to a typical retraction curve (top-right inset). These data are collected from time-course interference pattern changes. Data (crosses) are fitted with linear functions (lines). The slope of each fit allows for the determination of approach or retraction velocities.